

Supplementary Information

Identification of bridged CO₂ binding in a Prussian blue analogue using neutron powder diffraction

Stephen H. Ogilvie,^a Samuel G. Duyker,^b Peter D. Southon,^a Vanessa K. Peterson^b and Cameron J. Kepert*^a

^a Molecular Materials Group, School of Chemistry, The University of Sydney, NSW, 2006, Australia

^b Bragg Institute, Australian Nuclear Science and Technology Organisation, NSW, Australia

EXPERIMENTAL

Synthesis: Aqueous solutions of FeCl₂·H₂O (2.13 g, 10.72 mmol) and K₃Co(CN)₆ (1.69 g, 5.08 mmol) were mixed dropwise under vigorous stirring followed by aging for 24 h. The resultant precipitate was then filtered and washed with water (100 mL), followed by ethanol (100 mL) and dried in air to yield Fe₃[Co(CN)₆]₂ (1.7663 g). Activation of the sample was achieved by first grinding to a fine powder followed by dehydration in a glass sample tube at 423 K under high vacuum ($\sim 10^{-5}$ mbar).

X-ray powder diffraction (XRPD): Laboratory X-ray powder diffraction data were collected using the PANalytical X'Pert PRO MPD diffractometer (45.0 kV, 40.0 mA, 0.25° divergence, 7 mm anti-scatter slits) equipped with a copper anode that produced Cu-K α radiation ($\lambda = 1.5406 \text{ \AA}$). Data were collected over the 2 θ range 12.5 – 70°, with a 0.013° step size and 0.0355 °/s scan rate. The application software used was *X'Pert Data Collector v4.0*.¹

Thermogravimetric Analysis (TGA): Thermogravimetric analyses (TGA) were carried out using a TA Instruments Hi-Res TGA 2950 Thermogravimetric Analyser under a dry nitrogen atmosphere (flow rate of 0.1 L·min⁻¹). The sample was heated from 30 to 700 °C at a rate of 1 °C·min⁻¹.

Solid state Fourier transform infrared (FTIR) spectroscopy: Fourier transform infrared (FTIR) spectra were collected in a potassium bromide (KBr) matrix over the range 4000–400 cm⁻¹ using a Varian FTS-800 Scimitar series infrared spectrometer. Approximately 2–4 mg of material was combined with 200 mg of dried KBr by thoroughly grinding prior to data collection. A KBr background scan was obtained before each new scan and subtracted from the sample scan to obtain a difference spectrum.

Gas Adsorption: CO₂ adsorption isotherms were measured using a Hiden-Isochema IGA-002 gravimetric system. Freshly-prepared material was loaded into a stainless steel basket and heated to 95 °C under high vacuum (< 10⁻⁶ mbar) for 10 hr, by which point the mass was stable (approx. 48 mg). Isotherms were measured at 35, 40, and 45 °C, with the temperature maintained within 0.1 °C. The isotherms measured are shown in Fig S4. The kinetics of adsorption at pressures below 30 mbar were unusually slow, with the equilibrium mass not reached after an hour at each pressure. The mass gain was extrapolated using an Avrami equation to obtain an estimate of the equilibrium mass for plotting the isotherm; however, the uncertainties in these values were too high to be used in

the reliable determination of the enthalpy of adsorption at low loadings. There is a minor hysteresis between the adsorption and desorption arms, which we attribute, at least partially, to the slow kinetics.

Neutron powder diffraction: Neutron powder diffraction data were collected on the high-intensity neutron diffractometer, Wombat² (OPAL, Australia). Prior to neutron powder diffraction measurement and gas dosing, 0.816 g of anhydrous $\text{Fe}_3[\text{Co}(\text{CN})_6]_2$ was transferred to a cylindrical vanadium can (internal diameter of *ca.* 6 mm) inside a helium-filled glovebox equipped with water and oxygen monitors. The sample cell was connected to a custom-designed gas-delivery centrestick and inserted into a top-loading cryofurnace. Temperature control at the sample was achieved using cartridge heaters with silicon-diode temperature sensors at the top and bottom of the cell. The gas-delivery line was also temperature-controlled in order to avoid freezing CO_2 inside the tube, so that the sample could be left in place throughout the experiment without the requirement of warming the entire cryofurnace between gas doses. An initial diffraction pattern was collected on the evacuated sample at 15 K to be used as a structural reference point from which subsequent data for the CO_2 -dosed sample could be analysed. The sample was then warmed to 250 K prior to dosing with a known amount of CO_2 , before being slowly cooled to the measurement temperature of 15 K, all the while ensuring that the temperature was kept above the boiling/sublimation point of CO_2 at the current pressure. By 150 K the pressure reading was zero, indicating that all CO_2 had been absorbed by the sample. The total cooling time was approximately 1 hour, with the intention of ensuring diffusion of the CO_2 molecules to their thermodynamic equilibrium positions and minimising random disorder of guest molecules prior to the diffraction measurement. No evidence was found in the diffraction patterns that suggested any of the CO_2 was unaccounted for and, when coupled with the zero pressure reading, it was inferred that all of the CO_2 had been taken up by the sample framework. 30 min of diffraction data were acquired for each dose using an area detector in the angular range $17^\circ < 2\theta < 137^\circ$ with an incident neutron wavelength of 2.4145(3) Å, determined using an Al_2O_3 standard reference material (NIST SRM 676). A correction was applied to the Debye-Scherrer ring curvature before data reduction.

Structural Analysis.

Rietveld refinements were performed using GSAS³ through the EXPGUI⁴ interface. Prior to each Rietveld refinement, a Le Bail extraction was performed on each histogram to refine unit-cell parameters which were then kept constant during the Rietveld process. For gas-loaded samples, all reflections observed were able to be indexed in the $Fm\bar{3}m$ space group. The refined structure of the empty framework was used as a structural reference point from which subsequent structural information for the CO_2 -loaded sample was derived and refined. Following a Le Bail extraction to determine the unit cell parameters, the atom parameters for the empty framework were refined before Fourier-difference methods were used to extract CO_2 locations using the visualisation program VESTA. For subsequent CO_2 doses, two approaches for locating CO_2 were taken: 1) the refined model for the framework and initial dose of CO_2 was used as a starting point for each subsequent dose in order to determine any new guest locations, and 2) the model of the empty framework for every measurement was re-refined in order to ensure that an unbiased starting model for the framework itself was used. Comparison of these two methods revealed no discernible difference between results. The CO_2 -framework and CO_2 - CO_2 distances were considered in conjunction with site occupancy factors in order to ensure that physically-realistic results were obtained.

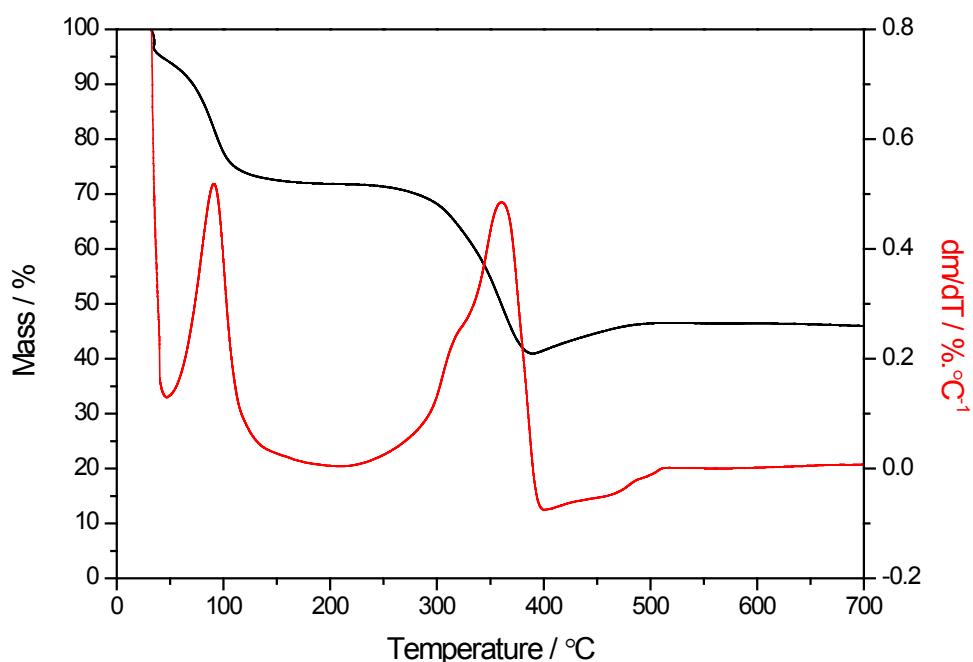


Fig. S1. Thermogravimetric analysis (TA, black) and derivative TA (red) of the $\text{Fe}_3[\text{Co}(\text{CN})_6]_2$ material from 30–700 °C. The immediate loss of *ca.* 5% mass at 30 °C is attributed to the loss of residual ethanol from washing. The 20% drop in mass between 75–100 °C demonstrates the loss of water molecules, both coordinated and uncoordinated, within the pores of the material. Decomposition of the material begins at *ca.* 280 °C.

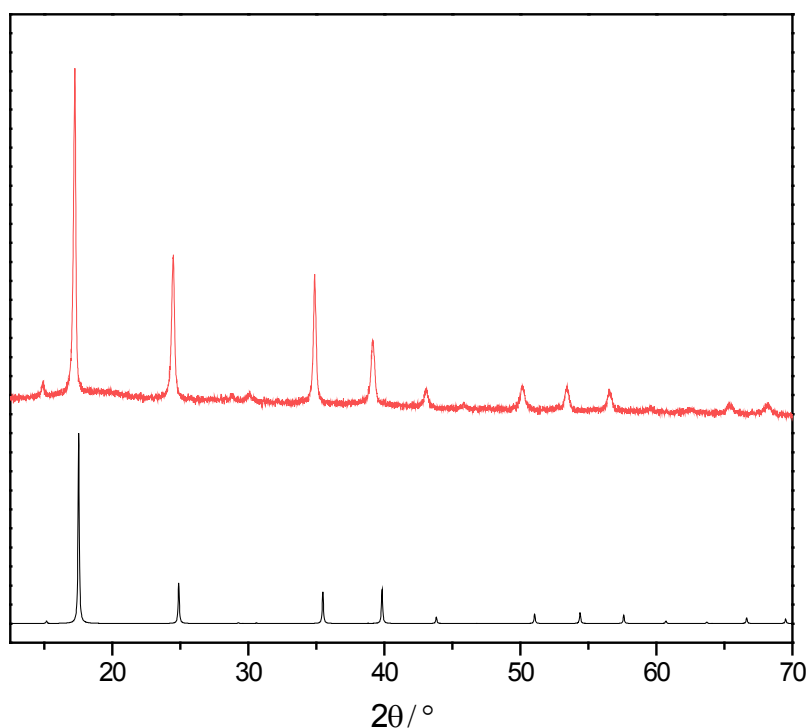


Fig. S2. Comparison of predicted (black line) and as-synthesised (red line) X-ray powder diffraction patterns for $\text{Fe}_3[\text{Co}(\text{CN})_6]_2$. Differences in intensity are attributed to the presence of water in the pores of the as-synthesised sample.

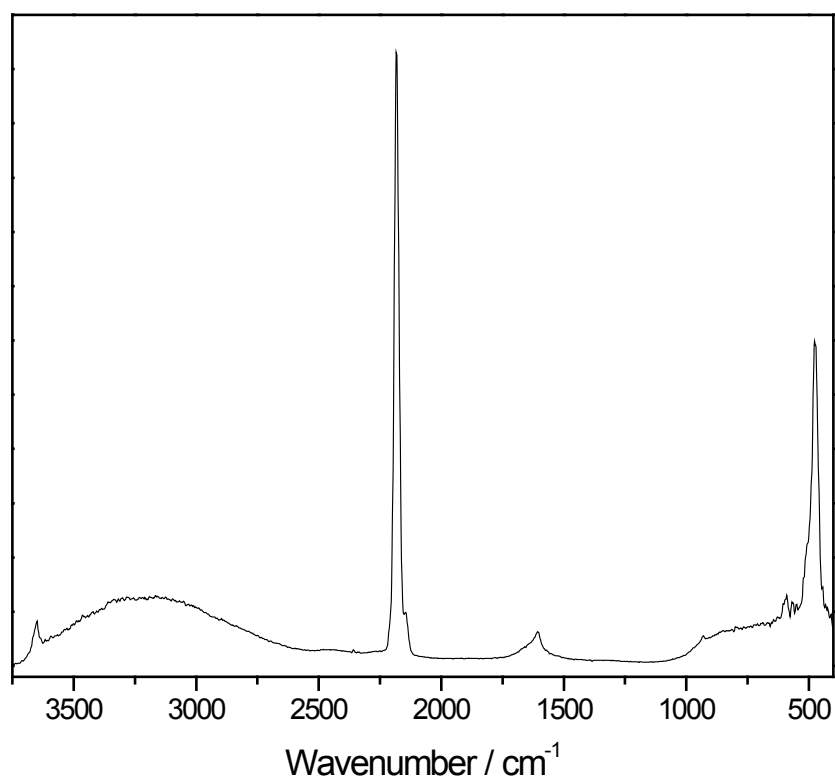


Fig. S3. FTIR spectrum of $\text{Fe}_3[\text{Co}(\text{CN})_6]_2$ demonstrating the cyanide longitudinal stretch at 2270 cm^{-1} . The broad band observed at 3200 cm^{-1} is attributed to the presence of water in the pores of $\text{Fe}_3[\text{Co}(\text{CN})_6]_2$.

DISTRIBUTION OF VACANCY PORES

Table S1: Distribution of vacancy-pores per 5 Å cubic pore as determined assuming a random distribution of vacancies.

Vacancies per 5 Å cubic pore	Probability formula	Probability (%)
0	$(2/3)^4$	19.8
1	$4 \times (1/3) \times (2/3)^3$	39.5
2	$6 \times (1/3)^2 \times (2/3)^2$	29.6
3	$4 \times (1/3)^3 \times (2/3)$	9.9
4	$(1/3)^4$	1.2

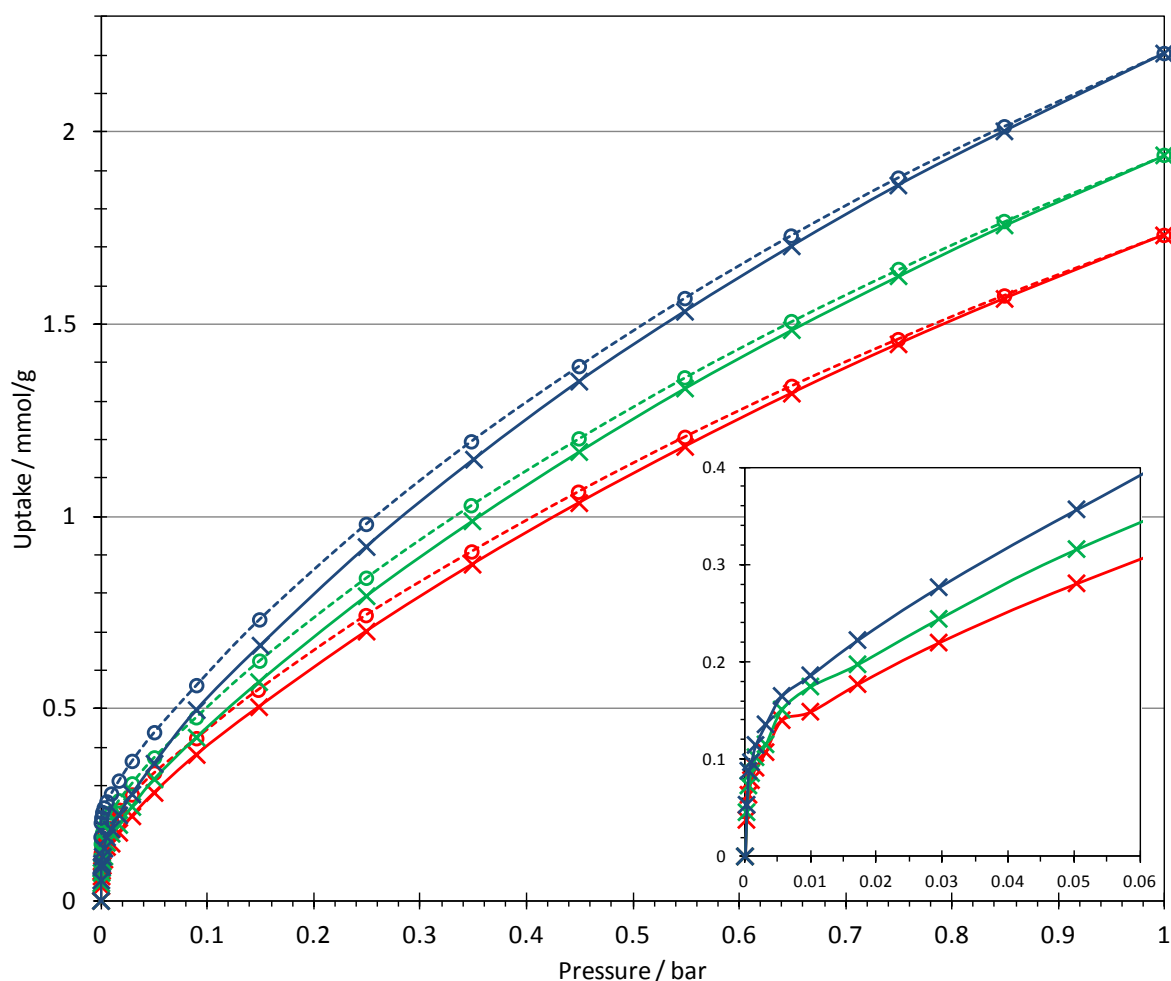


Fig. S4. Adsorption isotherms for CO_2 on $\text{Fe}_3[\text{Co}(\text{CN})_6]_2$ at 35, 40, and 45 °C (blue, green, and red, respectively). Adsorption data points are shown as crosses, desorption as circles.

NEUTRON POWDER DIFFRACTION ANALYSIS RESULTS

Table S2. Figure of merit (wR_p) of Rietveld refinements used to determine CO_2 quantities using neutron powder diffraction data for $\text{Fe}_3[\text{Co}(\text{CN})_6]_2$ and CO_2 -loaded $\text{Fe}_3[\text{Co}(\text{CN})_6]_2$.

Dosed $\text{CO}_2:\text{Fe}$	Unit cell $a = b = c$	Observed $\text{CO}_2:\text{Fe}$ Site A	Observed $\text{CO}_2:\text{Fe}$ Site B	Observed $\text{CO}_2:\text{Fe}$ total	wR_p (%)
0	10.1125(8)	0	0	0	3.32
0.49	10.1061(3)	0.572(29)	0.115(13)	0.687(42)	4.06
0.99	10.1068(9)	0.542(29)	0.559(14)	1.101(43)	3.6
1.49	10.1075(3)	0.566(25)	0.750(8)	1.316(33)	3.1

Neutron Powder Diffraction results: 0.49:Fe adsorption sites

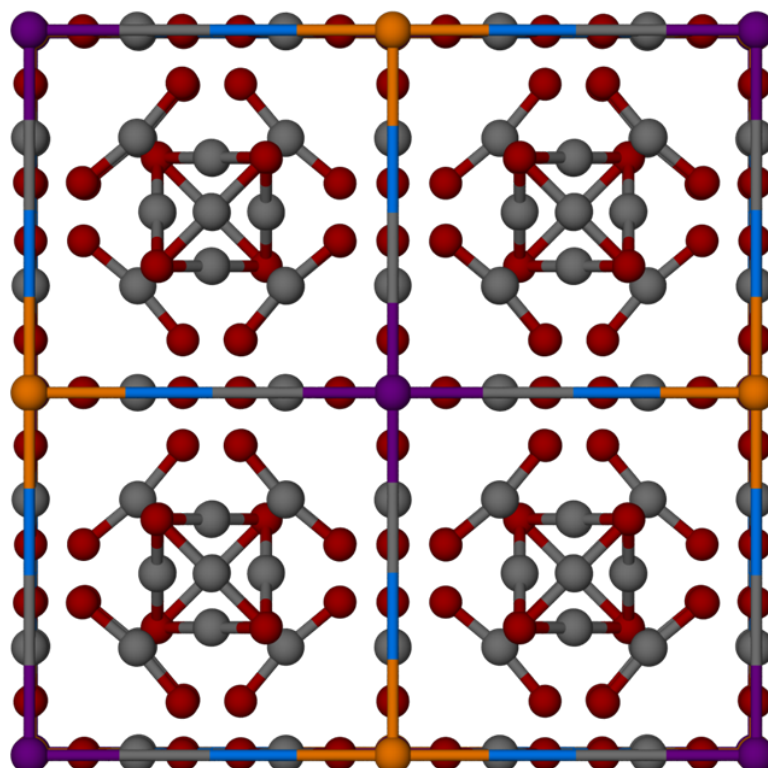


Fig. S5. View along the a -axis showing CO_2 sites A and B fully occupied in $\text{Fe}_3[\text{Co}(\text{CN})_6]_2$ with a CO_2 loading of 0.49 $\text{CO}_2:\text{Fe}$. Shown are cobalt (purple), iron (yellow), carbon (grey), nitrogen (light blue), and oxygen (red).

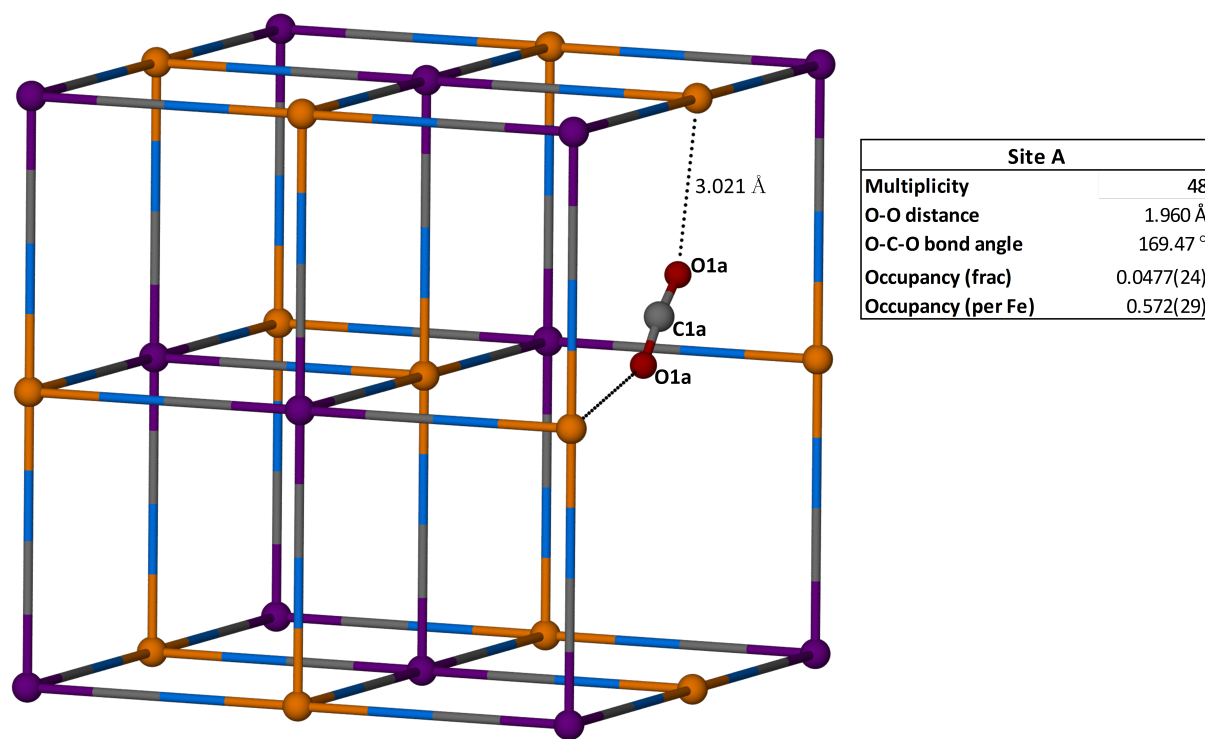


Fig. S6. Single CO₂ at adsorption site A at a CO₂:Fe, demonstrating proximity of the CO₂ molecule and the Fe₃[Co(CN)₆]₂ framework. Shown are cobalt (purple), iron (yellow), carbon (grey), nitrogen (light blue), and oxygen (red).

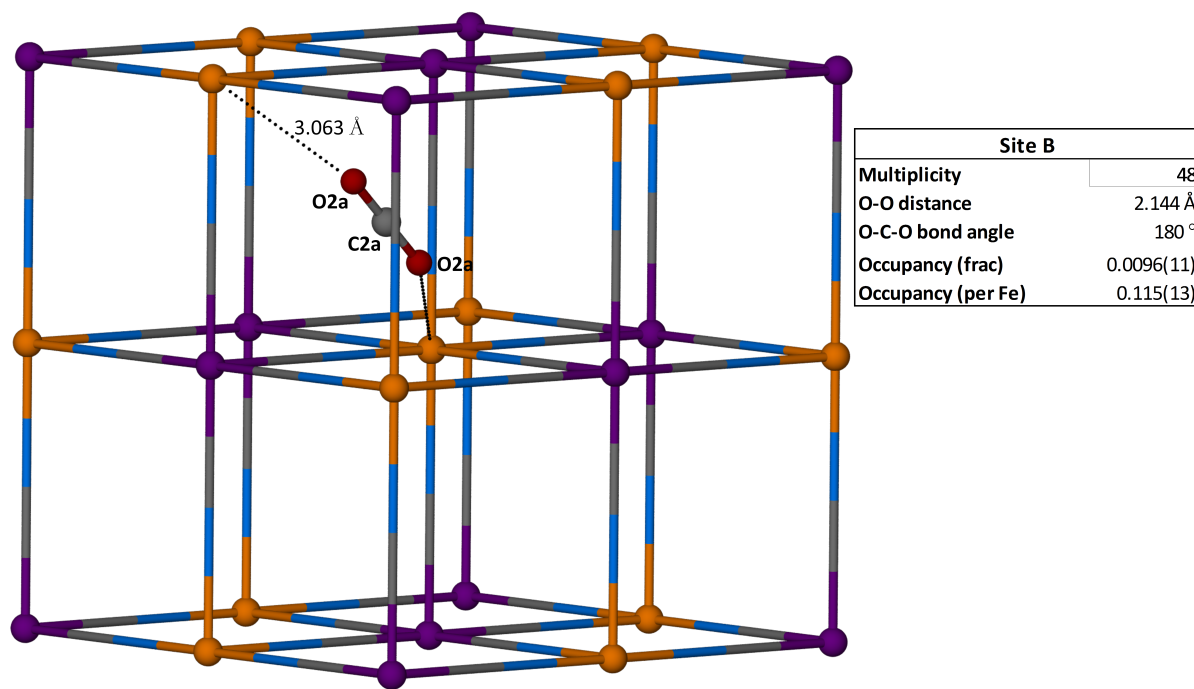


Fig. S7. Single CO₂ at adsorption site B at a CO₂:Fe demonstrating proximity of the CO₂ molecule and the Fe₃[Co(CN)₆]₂ framework. Shown are cobalt (purple), iron (yellow), carbon (grey), nitrogen (light blue), and oxygen (red).

Neutron Powder Diffraction results: 0.99 CO₂:Fe adsorption sites

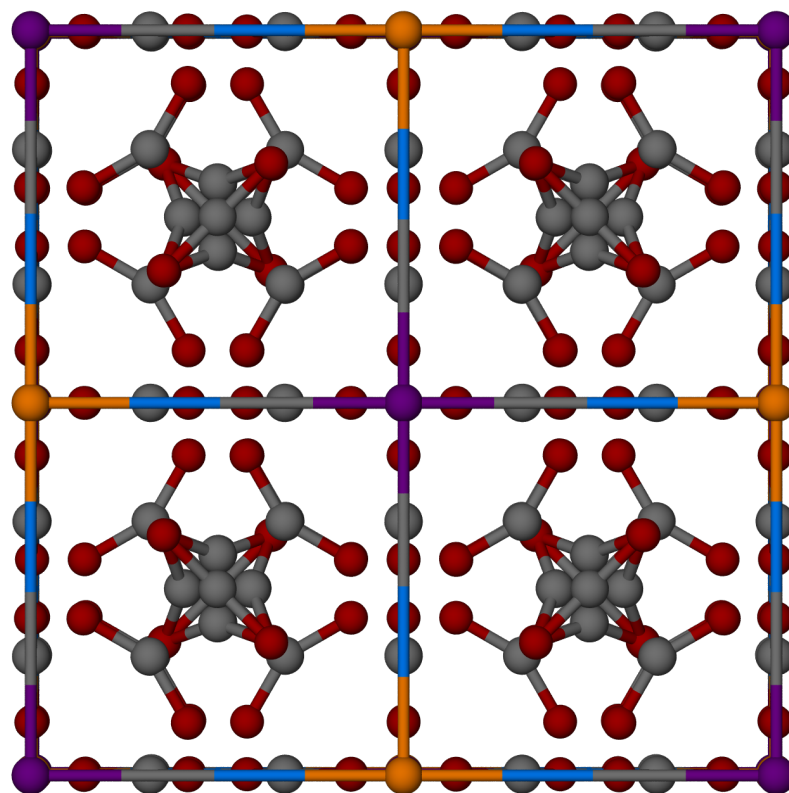


Fig. S8. View along the *a*-axis showing CO₂ sites A and B fully occupied in Fe₃[Co(CN)₆]₂ with a CO₂ loading of 0.99 CO₂:Fe. Shown are cobalt (purple), iron (yellow), carbon (grey), nitrogen (light blue), and oxygen (red).

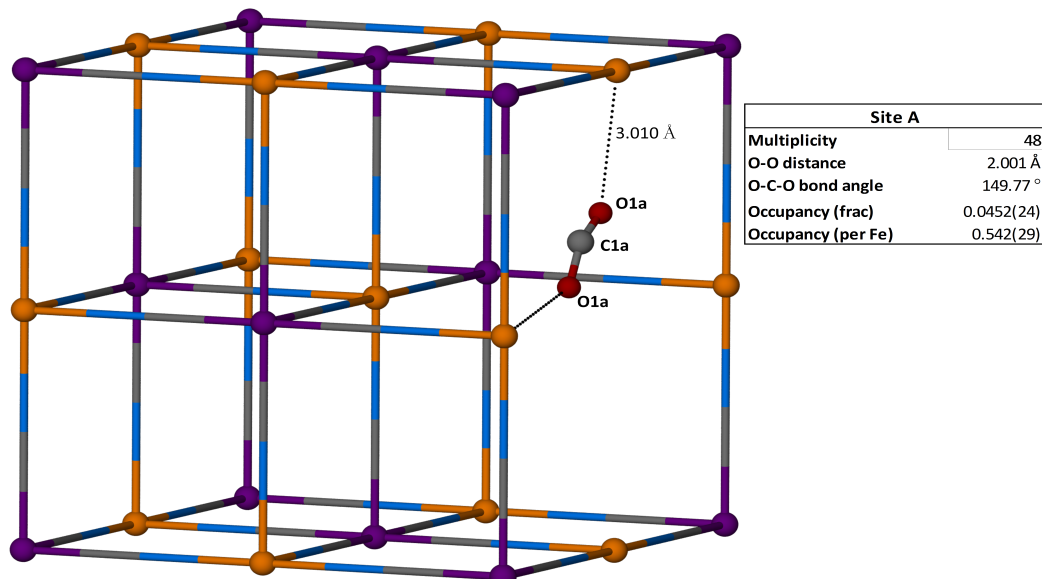


Fig. S9. Single CO₂ molecule at adsorption site A at a CO₂ loading of 0.99 CO₂:Fe CO₂:Fe demonstrating proximity of the CO₂ molecule and the Fe₃[Co(CN)₆]₂ framework. Shown are cobalt (purple), iron (yellow), carbon (grey), nitrogen (light blue), and oxygen (red).

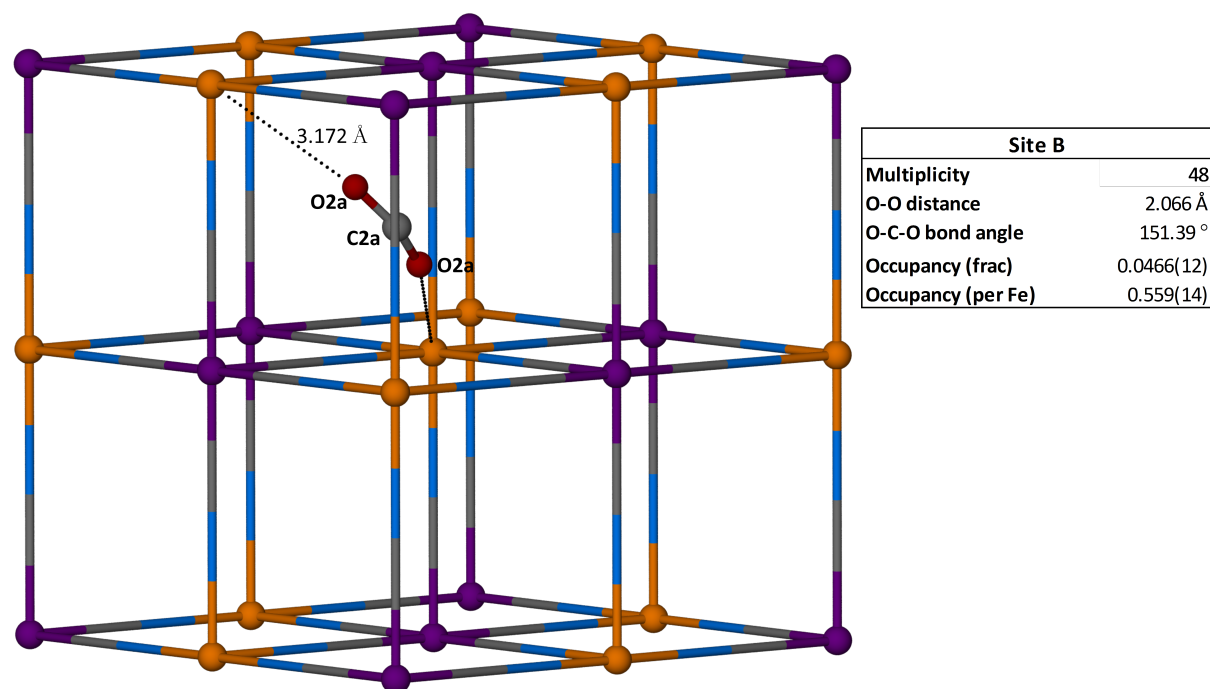


Fig. S10. Single CO₂ molecule at adsorption site B at a CO₂:Fe demonstrating proximity of the CO₂ molecule and the Fe₃[Co(CN)₆]₂ framework. Shown are cobalt (purple), iron (yellow), carbon (grey), nitrogen (light blue), and oxygen (red).

Neutron Powder Diffraction results: 1.49 CO₂:Fe adsorption sites

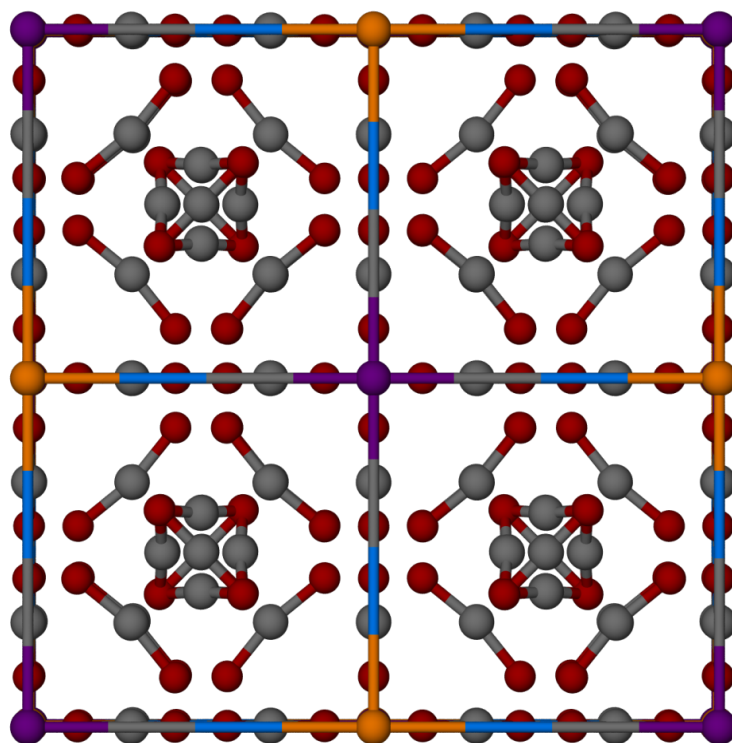


Fig. S11. View along the *a*-axis showing showing CO₂ sites A and B fully occupied in Fe₃[Co(CN)₆]₂ with a CO₂ loading of 1.49 CO₂:Fe. Shown are cobalt (purple), iron (yellow), carbon (grey), nitrogen (light blue), and oxygen (red).

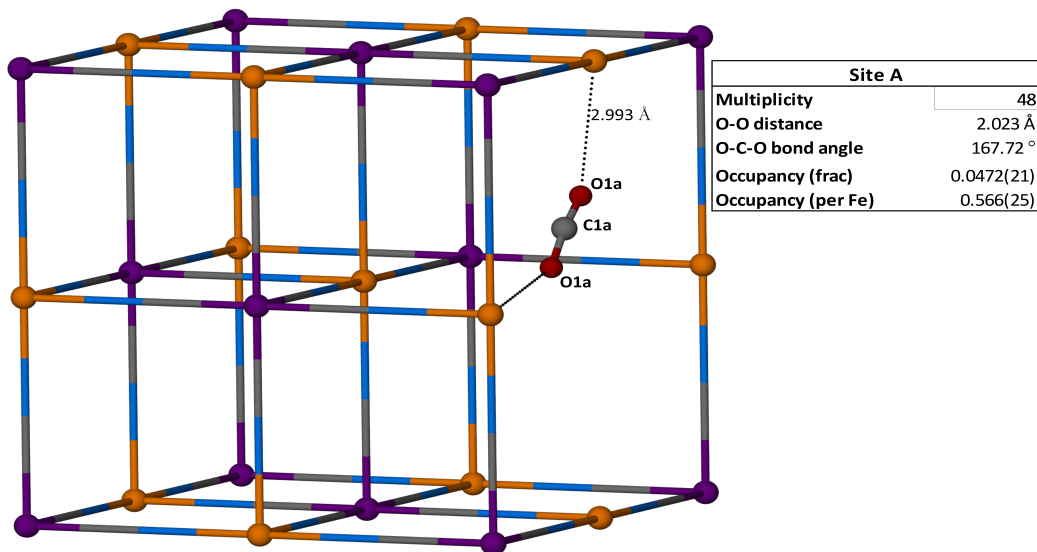


Fig. S12. Single CO₂ molecule at adsorption site A at a CO₂ loading of 1.49 CO₂:Fe demonstrating proximity of the CO₂ molecule and the Fe₃[Co(CN)₆]₂ framework. Shown are cobalt (purple), iron (yellow), carbon (grey), nitrogen (light blue), and oxygen (red).

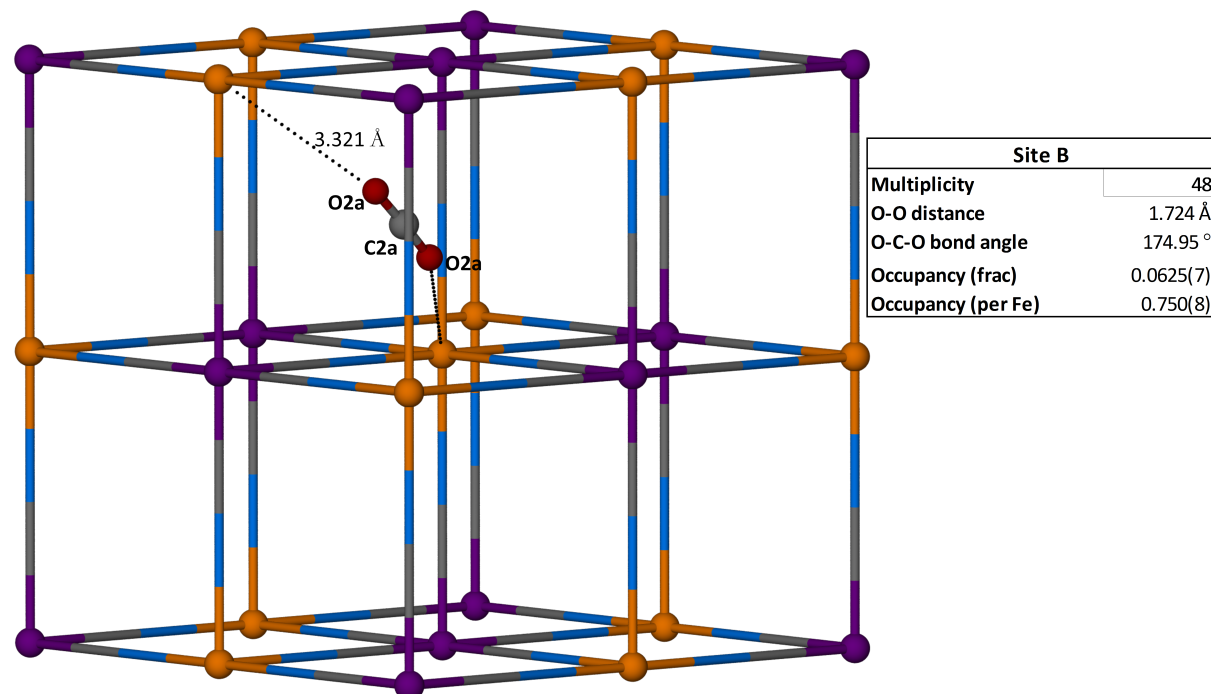


Fig. S13. Single CO₂ molecule at adsorption site B at a CO₂:Fe demonstrating proximity of the CO₂ molecule and the Fe₃[Co(CN)₆]₂ framework. Shown are cobalt (purple), iron (yellow), carbon (grey), nitrogen (light blue), and oxygen (red).

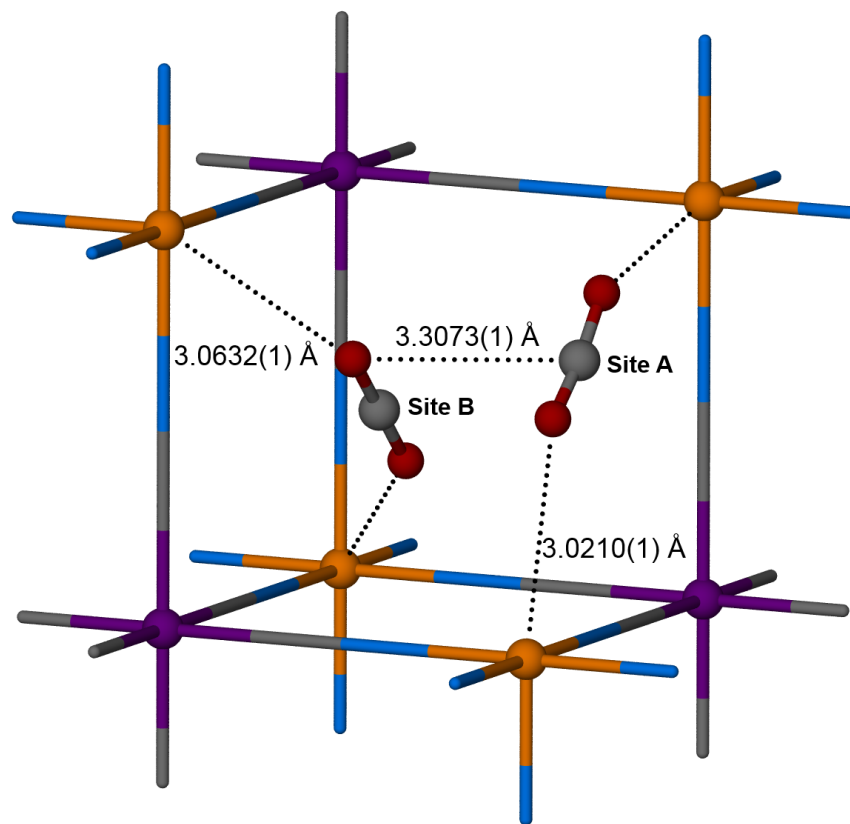


Fig. S14. Intermolecular interaction between neighbouring Site A and Site B CO_2 molecules within the vacancy pore of $\text{Fe}_3[\text{Co}(\text{CN})_6]_2$ at a loading of 0.49 $\text{CO}_2:\text{Fe}$ (*cf.* Fig. 2(b) of the manuscript, in which Site B is shown within the non-vacancy pore). Shown are cobalt (purple), iron (yellow), carbon (grey), nitrogen (light blue), and oxygen (red).

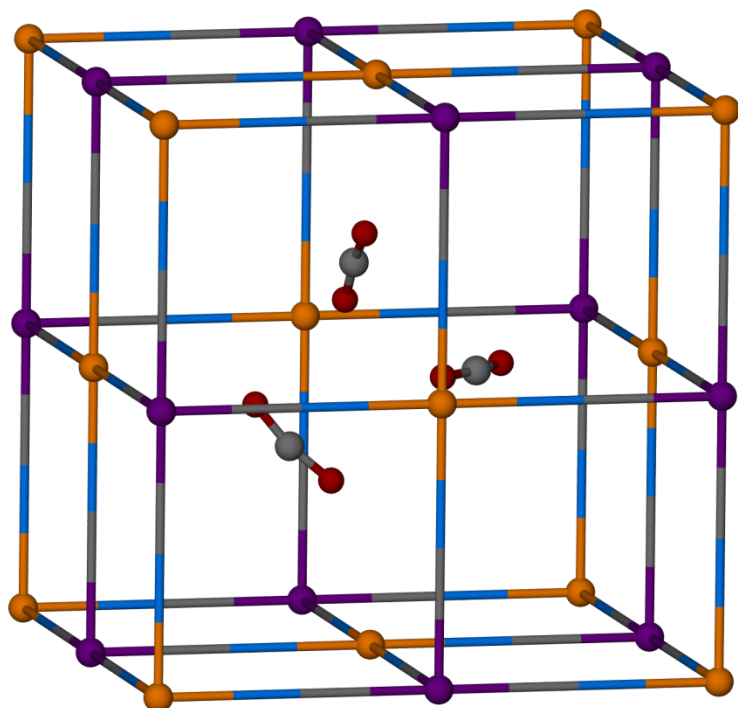


Fig. S15. A possible arrangement of three symmetrically equivalent CO₂ molecules at adsorption site A. This situation is geometrically analogous to tris-bidentate coordination about an octahedral metal centre (*cf.* planar bis-bidentate depicted in Fig. 3 of the manuscript). In this proposed configuration the C...O distance between neighbouring CO₂ molecules is *ca.* 3.4 Å. The observation of almost two rather than three site-A CO₂ molecules per vacancy suggests that the parallel arrangement of two CO₂ molecules is more favoured at the applied loading levels. Also possible is that occupation of two of the three A-sites shown occurs with some local distortion that makes loading of the third less favoured than loading of the neighbouring B-sites.

REFERENCES

1. *XPert Data Collector version 4.0*, PANalytical B.V., Almelo, The Netherlands.
2. A. J. Studer, M. E. Hagen and T. J. Noakes, *Physica B: Condensed Matter* (Amsterdam, Netherlands), 2006, **385-386**, 1013-1015.
3. R. B. Von Dreele and R. W. Larsen, *General Structure Analysis System*, Los Alamos National Laboratory, 2000.
4. B. H. Toby, *Journal of Applied Crystallography*, 2001, **34**, 210-213.